MECHANISMS OF TURBULENCE MODIFICATION IN DISPERSED TWO-PHASE FLOWS (TIME-RESOLVED PIV MEASUREMENTS OF INTERACTIONS BETWEEN PARTICLES/BUBBLES AND TURBULENCE)

Koichi Hishida and Yohei Sato
Department of System Design Engineering
Faculty of Science and Technology
Keio University
3–14–1 Hiyoshi, Kohoku-ku, Yokohama, 223–8522, JAPAN

ABSTRACT

Turbulence structure of dispersed two-phase flows has been investigated by particle image velocimetry (PIV) with a high time resolution using fluorescent tracer particles for phase velocity discrimination. The present study is confined to energy transport by solid particles in a turbulent channel flow and the effect of bubbles on fluid turbulence in an upward pipe flow.

A filtering technique was applied to the fluid flow amongst particles to extract a characteristic length scale that governs the energy transfer from particles to fluid turbulence. The turbulence intensity in the streamwise direction, which is identical to the gravity direction, was strongly augmented by particles whose size is slightly greater than the Kolmogorov length scale. The directional scale dependency structure was observed, i.e., large eddies were dissipated in front of particles and particle wake generated eddies, which is emphasized when particles aligned perpendicular to the gravity direction. The subgrid scale turbulence energy is increased until $\Delta/\eta \approx 10$ (Δ : filter width, η : Kolmogorov length scale), which means that particles generate eddies whose size is less than 10η. The energy backscatter in the presence of particles was observed at $\Delta/d_p \approx 5$ (d_p : particle diameter), indicating that particles affect the eddy motion whose size is approximately five times particle diameter

Turbulence modification in the presence of bubbles was investigated by using a PIV/LIF (laser induced fluorescence) system synchronized with a shadow imaging technique to detect the bubble's shape and position simultaneously. Turbulence energy was augmented by both large and small bubbles, which induced an increase in its dissipation rate. On the other hand, the Reynolds stress was strongly reduced in the whole region of pipe, yielding a decrease in the turbulence production. Energy forward/backscatter was significantly enhanced around bubbles, which means that the local vortex structure generated by bubbles may be responsible for the energy transport between large eddies to small ones, and the energy supply from bubbles motion.

INTRODUCTION

One of the most important aspects of dispersed two-phase flows is the interactions of solid particles or bubbles with turbulent flow fields. An increased understanding of the fundamental phenomena is required to ultimately improve the design of engineering devices in which these flows occur. Past experiments (e.g., Serizawa *et al.* 1975, Theofanous and Sullivan 1982, Fleckhaus *et al.* 1987, Lance and Bataille 1991, Rogers and Eaton 1991, Kulick *et al.* 1994, Sato *et al.* 1996) and numerical simulations (e.g., Squires and Eaton 1990, Elghobashi and Truesdell 1993, Sato and Hishida 1996, Boivin *et al.* 1998) have showed that turbulence attenuation or augmentation of continuous phase is dependent on the size of particle or bubble, the Reynolds number of particle or bubble and the volumetric ratio of dispersed phase to continuous one. However, the mechanisms responsible for this increase or decrease are still poorly understood.

To date the macroscale analyses present the following consensus interpretation. Gore and Crowe (1989*a*, 1989*b*) compiled data, foremost expressing the ratio of particle diameter to a characteristic length scale of the turbulence as a key parameter. They suggested that the critical value of the ratio separating regions of attenuation and augmentation was on the order of 0.1. Eaton (1994) reviewed past experiments and simulations in turbulence modification of simple flows and showed significant turbulence attenuation for mass loading ratios greater than 0.1. An outcome of these works revealed that the particle size and loading have a significant influence on turbulence modification.

The turbulence energy transport by particles was first examined by Sato and Hishida (1996) who introduced the multiple time-scale concept in their turbulence model. They indicated that large particles have a tendency to become clusters that affect large-eddy motion of fluid turbulence, which were supported by their experiments using particle image velocimetry (PIV), and uniformly-dispersed small particles dissipate turbulence kinetic energy, which induces energy cascade from small eddies to dissipative ones (Hishida and Sato 1999). For further insight into the nature

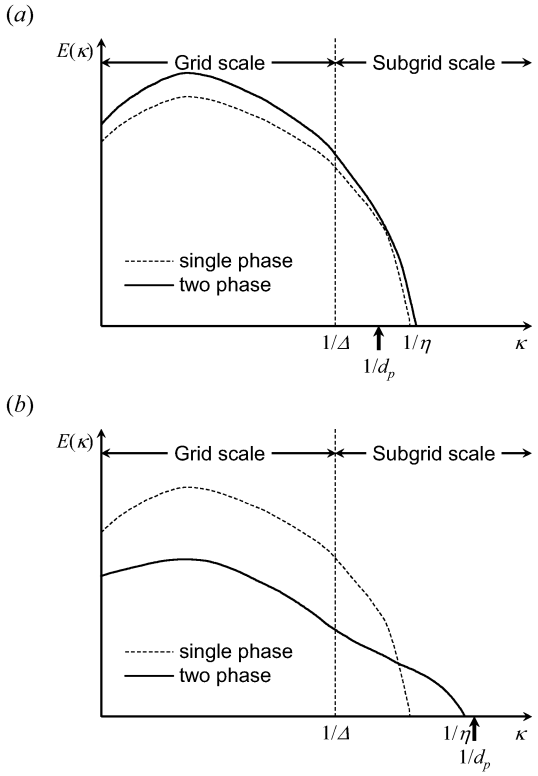

Figure 1. Schematic of turbulence modification by dispersed phase in wavenumber space. (*a*) Turbulence augmentation by large particles. (*b*) Turbulence attenuation by small particles.

of turbulence modification by dispersed phase, schematic of turbulence modification by particles in wavenumber space is exhibited in figure 1. For example, a cut-off filter is applied to divide energy power spectrum into grid scale and subgrid scale. None of the work, however, has revealed that the relationship between a filter size and the energy forward/backscatter due to particles. It's because that turbulence structure in figure 1(*a*) is completely different from that in figure 1(*b*). When large particles augment turbulence (figure 1(*a*)), turbulence energy is increased in the whole wavenumber region. On the other hand, a decrease in energy is observed except in high wavenumber region for the case of turbulence attenuation by small particles (figure 1(*b*)). One can reach a consensus on the relationship between the particle size and turbulence modification, however, the mechanisms of energy transfer between two phases is not fully resolved up to this day.

From the viewpoint of small-scale structure, the distortion process of fluid amongst particles in a vertical downflow water channel was investigated by Sato *et al.* (2000). Figure 2 shows time development of instantaneous maps of the rate of strain, the vorticity and image of the flow field detected by a CCD camera. They found directional scale dependency on turbulence augmentation using the inter-particle spacing, when the particle diameter is slightly greater than the Kolmogorov length scale. Sato *et al.* (2001) applied a filtering technique to fluid information amongst particles to investigate the energy backscatter by particles, which was reflected in modeling

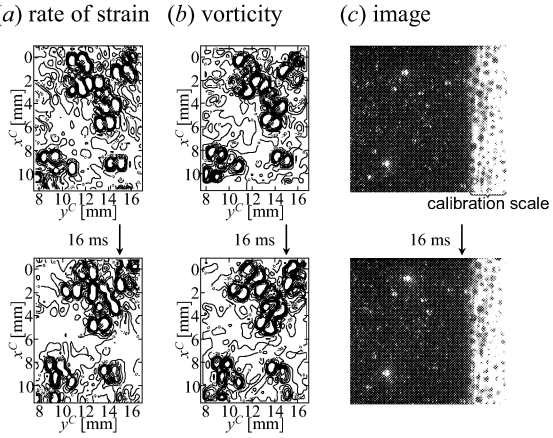

Figure 2. Time evolution of instantaneous maps of (*a*) the rate of strain, (*b*) the vorticity and (*c*) image of the flow field in the presence of 396 μm glass particles in a vertical downward channel flow (Sato *et al.* 2000).

directional scale dependency on force coupling in large eddy simulation (LES) (Inoue *et al.* 2001). The most important question, i.e., extracting a characteristic scale that governs energy transport by particles, has been explored by Sato and Hishida (2003) using filtered velocity fields.

To extend our understanding of the energy transport mechanisms in dispersed two-phase flows, the interactions between bubbles and fluid turbulence in a vertical upward pipe flow was investigated by using a high resolution PIV system (Minato *et al.* 2003, Yoshimura *et al.* 2004). They found a strong reduction in the Reynolds stress, inducing a decrease in the turbulence production. On the other hand, the dissipation rate of turbulence kinetic energy was enhanced in the whole region of pipe. However, the mechanisms of turbulence structure have not been fully discussed in their works.

The objective of the present study is to investigate the mechanisms of turbulence structure in dispersed two-phase flows by using PIV with a high time resolution. The experimental investigation focuses on

i) the interactions between fluid turbulence and solid particles in a vertical turbulent channel flow. A filtering technique, which is used in large eddy simulation, is applied to fluid information amongst particles to advance our understanding of energy forward/backscatter by particles.

ii) the interactions between bubbles and turbulence in a vertical pipe flow. A shadow imaging technique is employed to detect the bubble's shape and position, which is synchronized with a PIV system. The instantaneous structure around bubbles is captured by a high speed CMOS camera to understand how bubbles modify turbulence.

The important outcome obtained from the present set of experiments is to understand how particles or bubbles affect the energy cascade of fluid turbulence and specify a characteristic scale that governs the energy transfer from particles/bubbles to fluid turbulence.

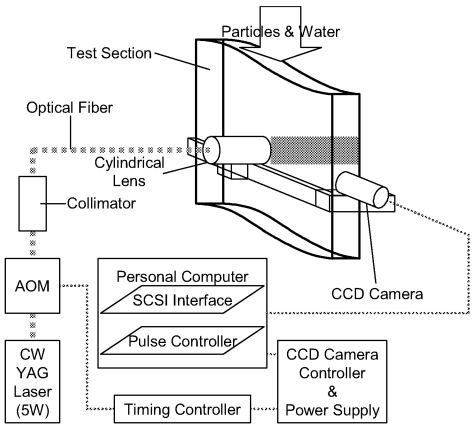

Figure 3. Schematic of particle image velocimetry and vertical water channel.

Table 1. Fluid flow parameters

Channel width	h	[mm]	30
Centerline mean velocity	$<U_c>$	[mm/s]	155
Channel Reynolds number	Re_h		5,740
Kinematic viscosity of water	ν	[mm^2/s]	0.81
Kolmogorov micro length scale†	η	[μm]	252
Kolmogorov micro time scale†	τ_K	[ms]	78.4

†value at channel centerline

Table 2. Properties of particles

Material			glass
Number mean diameter	d_p	[μm]	396.4
Stan. dev. of diameter	σ_p	[μm]	32.3
Density	ρ_p	[kg/m^3]	2,590
Terminal velocity	V_t	[mm/s]	102
Particle time constant	τ_p	[ms]	10.4
Particle Reynolds number‡	Re_p		50.0
Particle mass loading ratio	ϕ_{mass}		3.3×10^{-4}, 8.6×10^{-4}
Particle volumetric fraction	ϕ_{vol}		1.8×10^{-4}, 3.3×10^{-4}

‡mean value calculated by using instantaneous particle Reynolds number

ENERGY TRANSPORT BY SOLID PARTICLES IN A TURBULENT CHANNEL FLOW

Experimental setup

The present experiments were performed in a two-dimensional, vertical channel with downflow of water, identical to that of Sato *et al.* (2000, 2001), as shown in figure 3. The channel was vertically oriented so that the gravitational force on the particles was aligned with the direction of flow. Boundary-layer trips were affixed to both walls at the entrance of a 1.0 m long, 30×250 mm test section. Some of the properties of the flow are presented in table 1. All the experiments were run at a centerline mean velocity of 155 mm/s, corresponding to a Reynolds number of 5,740 based on channel width. The temperature of water was kept constant by using a heater to avoid varying fluid properties. The Kolmogorov micro length scale, η, at the channel centerline was 252 μm, which was calculated by direct measurements of dissipation rate of turbulence kinetic energy.

Glass particles were used in the present set of experiments and their characteristics are compiled in table 2. The particle size was chosen with the following strategy: (i) smaller than the energy-containing scale of the flow (l_e = 1.6 mm at the channel centerline) and (ii) slightly greater than the Kolmogorov micro scale of turbulence. The particle size distributions were determined by using successively smaller sieves, while the particle sphericity was checked by using a microscope. The particle volumetric fraction is less than 5.0×10^{-4} (Rizk and Elghobashi 1989), so that the inter-particle collision is neglected.

Velocities of both phases were obtained by using PIV developed by Sato *et al.* (2000, 2001). Figure 3 shows a schematic illustration of a PIV system. Velocities were calculated by a cross-correlation technique between two images. Polyethylene particles of 5 μm (density of 960 kg/m^3) were added as tracer particles to the liquid phase. The thickness of the YAG-laser light sheet was 3.0 mm in the test section.

The measurement uncertainty in these experiments was 2.0% for instantaneous velocity measurements. The particles and surrounding fluid were measured by a high speed CCD camera (Kodak Motion Corder Analyzer SR-500, 512×512 pixels) in a matter of few seconds. Subsequently velocities in time series were calculated within an interval of 1/125 s (= 8 ms). Measurements in both *XY* and *XZ* planes were carried out by exchanging the position of CCD camera for the optical system.

Properties of the flow field

Figure 4 shows profiles of the mean streamwise velocity of water in the presence of particles. The coordinate of the figure has nondimensionalized values based on the centerline mean velocity in single phase, $<U_c>$, of 155

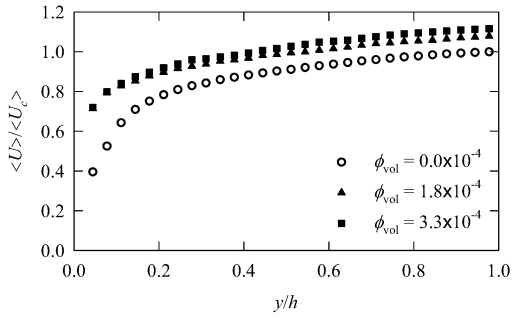

Figure 4. Profiles of mean streamwise velocity of water in the presence of particles.

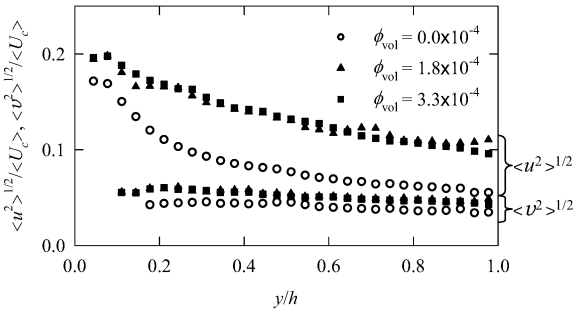

Figure 5. Profiles of fluctuating streamwise and transverse velocity of water in the presence of particles.

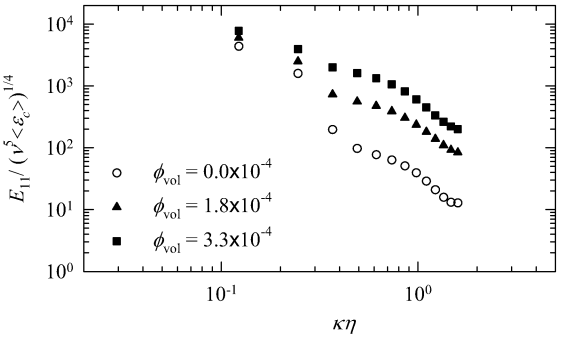

Figure 6. Profiles of streamwise velocity power spectrum of water at the channel centerline in the presence of particles.

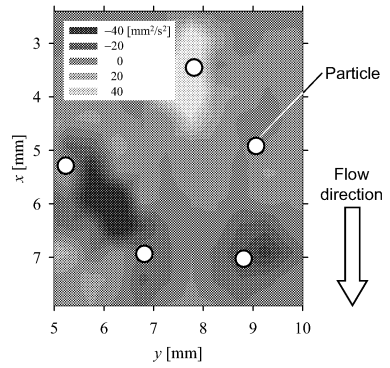

Figure 7. Contour plot of the *real* SGS stress element, τ_{12}, computed with the top-hat filter of $\Delta = 0.5$ mm.

mm/s and a channel width, h, of 30 mm. It is observed that the mean fluid velocity was accelerated with an increase in the volumetric fraction, because the falling particles accelerated the surrounding fluid at the constant pressure gradient. Streamwise fluctuating velocity, as shown in figure 5, was significantly augmented by particles in comparison with transverse fluctuating velocity. This is supported by figure 6 that exhibits profiles of streamwise velocity power spectrum of water at the channel centerline, which is calculated by

$$E_{ii}(\kappa) = \int_0^{T\langle U_i\rangle} \left| u_i\left(t\langle U_i\rangle\right) e^{-i\kappa\left(t\langle U_i\rangle\right)} \right|^2 d\left(t\langle U_i\rangle\right). \quad (1)$$

The ordinate is normalized by kinematic viscosity of water, ν, and dissipation rate of turbulence kinetic energy of water, $<\varepsilon_c>$, in single phase, while the abscissa is normalized by the Kolmogorov micro length scale of water, η, in single phase. An increase in turbulence energy in the high wavenumber region was observed with an increasing value of particle volumetric fraction, which is identical to the conclusions obtained by Hishida and Sato (1999).

Basic statistics of SGS stress

Further insight into extracting a characteristic scale that governs energy transport by particles is provided by using a filtering technique. The filtered velocity field, $\overline{u}_i$, is formally defined as

$$\overline{u}_i(x_i, x_j) = \int_{-\infty}^{\infty}\int_{-\infty}^{\infty} G(x_i - x_i', x_j - x_j') u_i(x_i', x_j') dx_i' dx_j', \quad (2)$$

where $G(x_i,x_j)$ is a spatial low-pass filter with a characteristic width, Δ. A top-hat filter is applied to fluid information amongst particles obtained from PIV measurements, which is defined as

$$G(x_i, x_j) = \begin{cases} c_G & \text{if } |x_i| < \frac{1}{2}\Delta \text{ and } |x_j| < \frac{1}{2}\Delta, \\ 0 & \text{otherwise} \end{cases} \quad (3)$$

where the coefficient c_G is a normalization factor which ensures that the integral of the filter equals unity (in the discrete sense).

The SGS stress element, τ_{ij}, and the filtered strain rate, $\overline{S}_{ij}$, are defined as

$$\tau_{ij} = \overline{u_i u_j} - \overline{u}_i \overline{u}_j, \quad (4)$$

$$\overline{S}_{ij} = \frac{1}{2}\left(\frac{\partial \overline{u}_i}{\partial x_j} + \frac{\partial \overline{u}_j}{\partial x_i}\right). \quad (5)$$

Figure 7 displays contour plot of the *real* SGS stress (Liu *et al.* 1994, 1999) obtained from PIV measurements computed with the top-hat filter of $\Delta = 0.5$ mm, which is nearly equal to the particle diameter, d_p. It is observed that both positive and negative values are appeared around particles, which is also found in the results from *XZ*-plane measurements.

Energy transport by particles

Turbulence energy in grid scale (GS) and subgrid scale (SGS) in dispersed two-phase flows will advance our understanding of energy cascade from large eddies to small ones in the presence of particles. The GS and SGS turbulence energy is defined as

$$k_{GS} = \frac{1}{2}\overline{u}_k \overline{u}_k, \quad (6)$$

$$k_{SGS} = \frac{1}{2}\left(\overline{u_k u_k} - \overline{u}_k \overline{u}_k\right). \quad (7)$$

The transport equation of k_{GS} and k_{SGS} takes on the form,

$$\frac{\partial k_{GS}}{\partial t} + \overline{u}_j \frac{\partial k_{GS}}{\partial x_j} = -\Pi_{ij} - \varepsilon_{GS} + \frac{\partial}{\partial x_j}\left(-\overline{u}_i \tau_{ij} - \overline{p u}_j + \nu \frac{\partial k_{GS}}{\partial x_j}\right) - \overline{\varepsilon}_{p,GS}, \quad (8)$$

$$\frac{\partial k_{SGS}}{\partial t} + \overline{u}_j \frac{\partial k_{SGS}}{\partial x_j} = \Pi_{ij} - \varepsilon_{SGS} + \frac{\partial}{\partial x_j}\left[-\overline{u}_i \tau_{ij} - \frac{1}{2}\left(\overline{u_i u_i u_j} - \overline{u}_j \overline{u_i u_i}\right) - \left(\overline{p u_j} - \overline{p u}_j\right) + \nu \frac{\partial k_{SGS}}{\partial x_j}\right] - \overline{\varepsilon}_{p,SGS}, \quad (9)$$

where Π_{ij} is energy flux to unresolved scales, which is defined as

$$\Pi_{ij} = -\tau_{ij}\overline{S}_{ij}. \quad (10)$$

Figures 8 and 9 depict contour plot of k_{GS}, k_{SGS} and Π calculated by using the top-hat filter of $\Delta = 0.75$ mm (≈

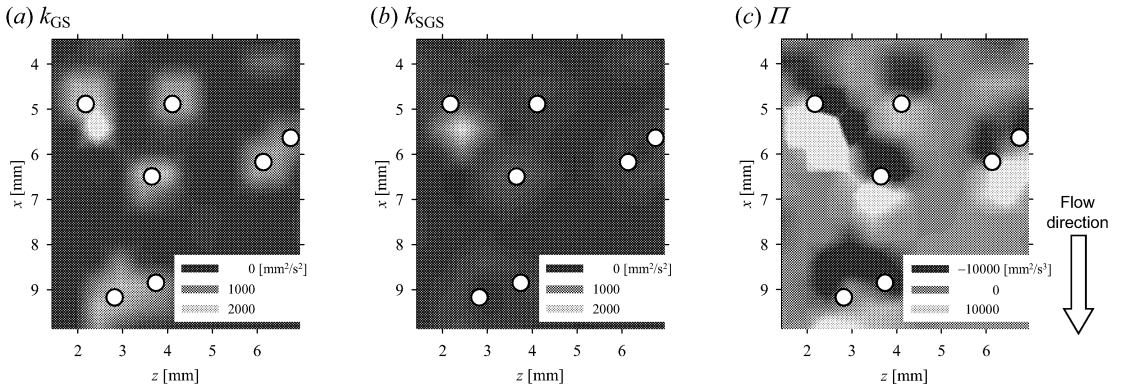

Figure 8. Contour plot of (*a*) turbulence energy in grid scale, k_{GS}, (*b*) turbulence energy in subgrid scale, k_{SGS}, and (*c*) energy flux to subgrid scale, Π, computed with the top-hat filter of $\Delta = 0.75$ mm ($\approx 2d_p$).

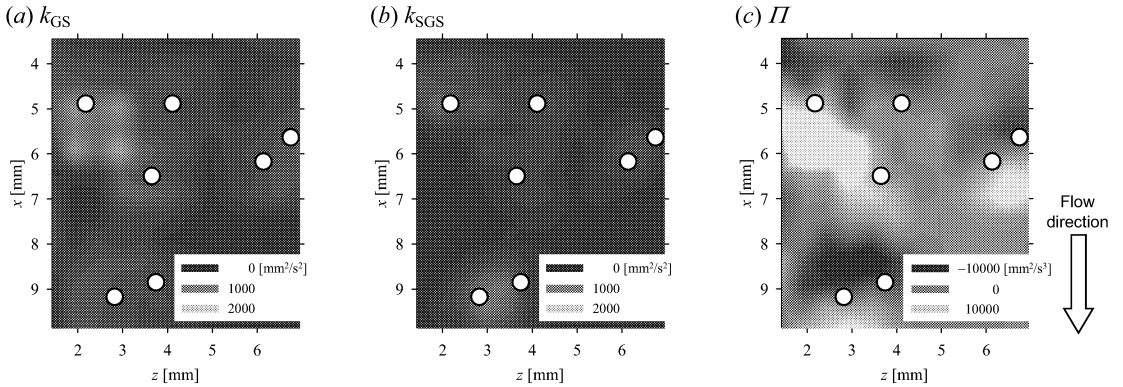

Figure 9. Contour plot of (*a*) turbulence energy in grid scale, k_{GS}, (*b*) turbulence energy in subgrid scale, k_{SGS}, and (*c*) energy flux to subgrid scale, Π, computed with the top-hat filter of $\Delta = 2$ mm ($\approx 5d_p$).

$2d_p$) and $\Delta = 2$ mm ($\approx 5d_p \approx l_e$), respectively. It is obvious from figures 8(*a*) and 9(*a*) that narrower the filter width is, larger k_{GS} around particles becomes. On the other hand, from figures 8(*b*) and 9(*b*), wider the filter width is, larger k_{SGS} amongst particles becomes. It means that the relationship between the filter width and the inter-particle spacing should be considered in the SGS model of LES (Inoue *et al.* 2001). Moreover, when particles aligned perpendicular to the gravity direction, k_{GS} has large values amongst particles as shown in figure 8(*a*), in which the inter-particles spacing, l_p, is estimated to be $l_p \approx 0.3l_e$–$0.5l_e$ or $l_p \approx d_p$–$0.5d_p$. It is found from figure 8(*c*) that there exist positive value regions of Π in front of particles, while negative regions behind particles. This result indicates that large eddies are dissipated in front of particles, on the other hand, particle wake generates eddies. It can be concluded that, from the viewpoint of small scale, the interactions between both phases show the directional scale dependency structure, which controls the energy transfer from large eddies to small ones affected by particles.

The GS and SGS turbulence energy as a function of filter width is plotted in figure 10 in order to extract a characteristic length scale that governs the energy transport by particles. The ordinate is normalized by the turbulence kinetic energy in single phase at the channel centerline, $<k_c>$, while the abscissa is normalized by the Kolmogorov micro length scale, η. Both turbulence energies were calculated by using approximately 0.16 million statistics from 2,000 pairs of images. In single phase the SGS

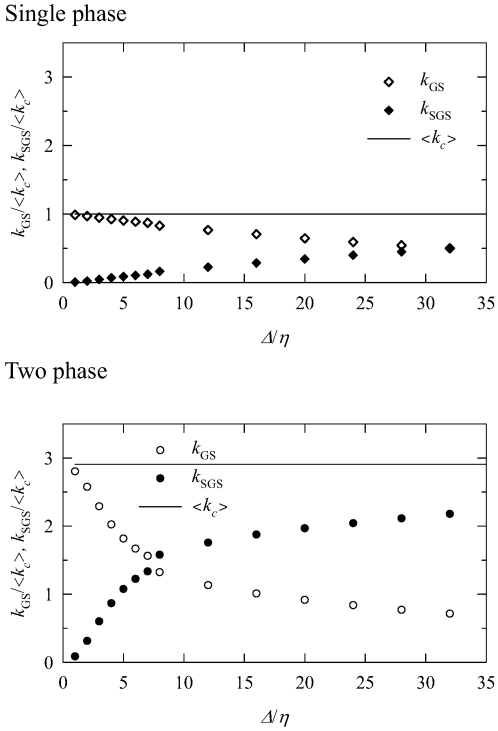

Figure 10. Profiles of turbulence energy in grid scale and subgrid scale (*a*) in single phase and (*b*) in the presence of particles at $\phi_{vol} = 3.3\times10^{-4}$.

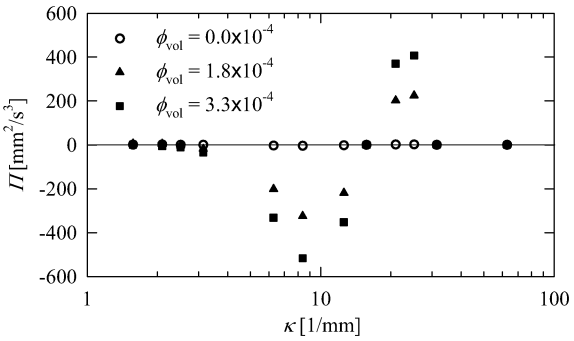

Figure 11. Profiles of energy flux to subgrid scale by particles in wavenumber space computed with the cut-off filter.

turbulence energy takes a zero value at $\Delta/\eta = 1$ and is increased with increasing values of the filter width. On the other hand, in the presence of particles the SGS turbulence energy is rapidly increased until $\Delta/\eta \approx 9$ and becomes larger than that in GS at $\Delta/\eta \approx 8$. This means that particles generate eddies whose size, l, is over the range of $\eta < l \leq 10\eta\,(\approx 5d_p)$.

Direct numerical simulation is a powerful tool to investigate the effect of particles on the energy cascade from large eddies to dissipative ones (Elghobashi and Truesdell 1993), however, the result remains restricted to relative low Reynolds and homogeneous turbulent flows. The present study focuses on the energy forward/backscatter by particles by applying the cut-off filter to fluid information amongst particles. Figure 11 shows profiles of energy flux to subgrid scale in the presence of particles as a function of wavenumber. At $\kappa \approx 20$ ($2\pi/d_p \approx 24$) the sign is reversed, that is, the particles supply the energy to small eddies whose size is less than the particle diameter, while the energy backscatter occurs in large eddies.

It is concluded that the energy transport by particles is dependent on the directional scale dependency structure in which particles generate eddies whose size is less than 10η and affect the eddy motion whose size is approximately five times particle diameter, which is identical to the conclusion obtained by Sato *et al.* (2000, 2001).

INTERACTIONS BETWEEN BUBBLES AND TURBULENCE IN AN UPWARD PIPE FLOW

Experimental setup

The present experiments were performed in a vertical pipe with upflow water (Minato *et al.* 2003, Yoshimura *et al.* 2004), as shown in figure 12(*a*). At the bottom of pipe, a bubble generator and a honeycomb for rectifying an incoming flow were located. Tap water was flowed in the pipe at the entrance of a 1.5 mm long, the internal diameter of 44 mm test section. An FEP (fluorinated ethylene propylene copolymer) pipe was selected in the test section to avoid optical distortion due to refraction from the pipe. The refractive index of FEP, 1.338, is approximately the same as that of water, 1.332. Some of the properties of the flow are presented in table 3. All the experiments were run at a bulk mean velocity of 196 mm/s, corresponding to a Reynolds number of 9,700 based on pipe diameter. The

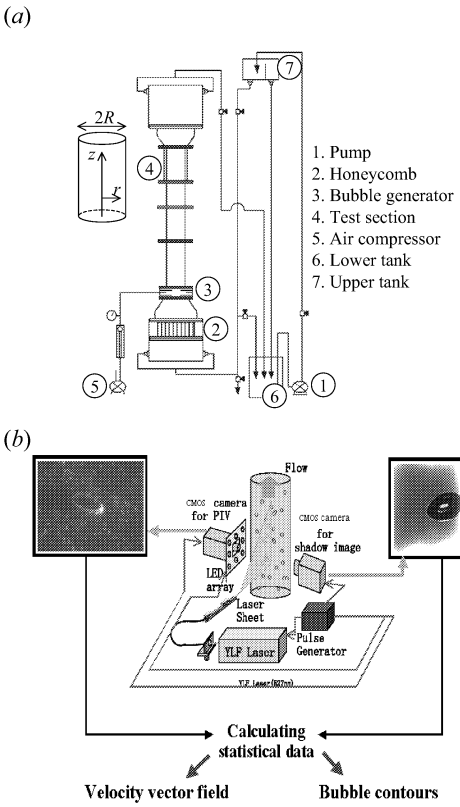

Figure 12. Schematic of (*a*) experimental apparatus and (*b*) measurement system.

Table 3. Fluid flow parameters

Pipe diameter	$2R$	[mm]	44
Centerline mean velocity	$\langle U_c \rangle$	[mm/s]	230
Bulk mean velocity	$\langle U_b \rangle$	[mm/s]	196
Pipe Reynolds number	Re_{2R}		9,700
Kolmogorov micro length scale§	η	[μm]	300
Kolmogorov micro time scale§	τ_K	[ms]	70
Void fraction	α	[%]	0.5

§value at pipe centerline

present study focuses on the effect of bubble diameter on turbulence modification, so that 3-pentanol ($C_5H_{11}OH$) was added to water as surfactant in order to reduce the bubble diameter.

Velocities of both phases were obtained by using a PIV system as illustrated in figure 12(*b*). Two CMOS cameras (IDT X-Stream XS-3, 1284 × 1024 pixels) were used: a left camera in figure 12(*b*) is for PIV/LIF (laser induced fluorescence) and a right one for detecting bubble shape. A square "window" array of LEDs permitted a view for PIV/LIF. Light reflected from bubbles, which was approximately thousand times that from tracer particles, saturated the CMOS device and overwhelmed the signal of tracer particles (Tokuhiro *et al.* 1998), therefore it is difficult to detect the tracer particles in the vicinity of bubbles. A LIF technique was applied by using fluorescent tracer particles, into which methyl-methacrylate ($H_2C{=}C(CH_3)COOCH_3$) with Rhodamine B was impregnated. An YLF laser (Quantronix Falcon 527DP, 15 mJ/pulse, λ = 539 nm) was used as a light source in this

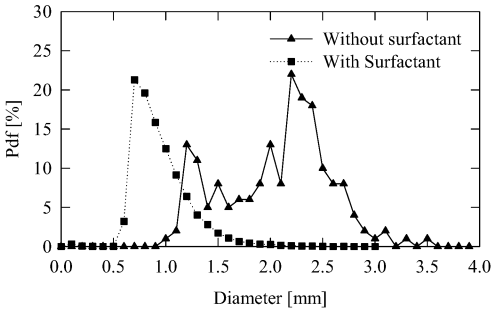

Figure 13. Bubble diameter distribution.

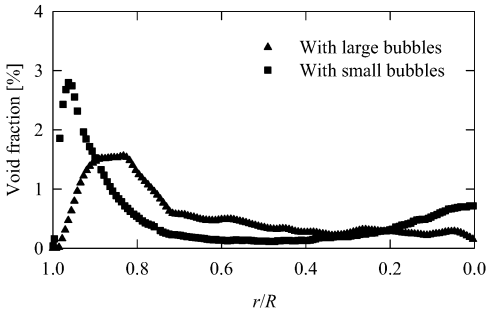

Figure 14. Profiles of local void fraction.

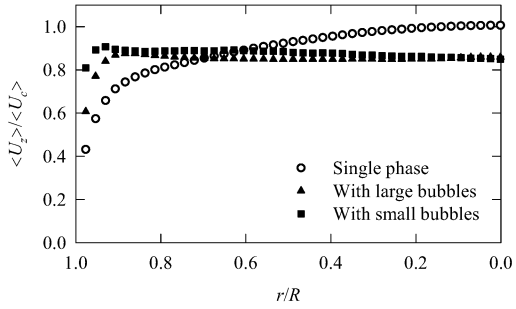

Figure 15. Profiles of mean streamwie velocity of water in the presence of bubbles.

measurement system. Fluorescence from the tracer particles was detected through a color filter by using a left camera.

A projection technique using blue LEDs (λ = 473 nm) was employed as a light source to capture the bubble shape and position simultaneously. A bubble image in grayscale is depicted in the right-hand side of figure 12(*b*). The focal depth of the CMOS camera is approximately 6 mm, so that an instant of continuous oscillated motion was captured in this field. The emitted light passed through a filter attached to the CMOS camera that recorded both the shadow image and a blue light. The frame rate and the image size of two cameras were set at 500 Hz and 600×900 pixels, respectively. The measurement uncertainty in these experiments was 2.0% for instantaneous velocity measurements.

Properties of the flow field

The bubble diameter was evaluated by using shadow images projected onto the CMOS camera. Figure 13 shows distribution of the equivalent bubble diameter with and

(*a*) Streamwise direction

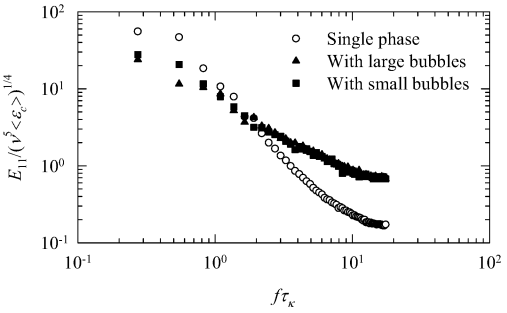

(*b*) Transverse direction

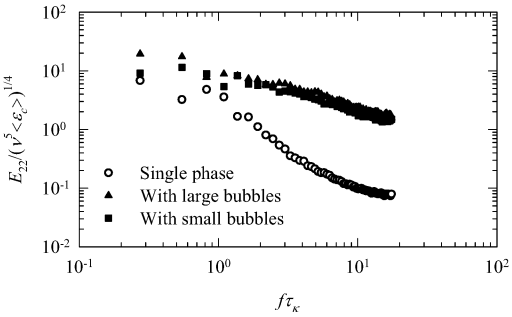

Figure 16. Profiles of (*a*) streamwise and (*b*) transverse power spectrum of water at the pipe centerline in the presence of bubbles.

without 3-pentanol. The bubble diameter took a peak value of 0.9 mm with surfactant, while 2.0 mm without surfactant. In the present study the experiments with and without surfactant are hereinafter referred to with small and large bubbles, respectively.

The local void fraction for each case was obtained by projected images of bubble shape that was captured within a thin focal depth, as shown in figure 14. The abscissa is normalized by a pipe radius, R, of 22 mm. The local void fraction is defined as the ratio of bubble volume to measurement one. It is found that bubbles have a tendency to accumulate near the wall for both cases due to the lift force acting on bubbles.

Figure 15 shows profiles of the mean streamwise velocity of water in the presence of bubbles. The ordinate is normalized by the centerline mean velocity in single phase, $<U_c>$, of 230 mm/s. It is obvious that the mean fluid velocity near the wall was accelerated for both cases, inducing the flat velocity profile. The bubbles ascending near the wall have a significant influence on the streamwise velocity due to their buoyancy. It can be seen from figures 14 and 15 that the both the local void fraction and mean velocity had a peak value at $r/R \approx 0.95$.

Interactions between bubbles and fluid turbulence

Fluid power spectra in the presence of bubbles were obtained by using 1,024 images to investigate effects on bubbles on turbulence modification. Figure 16 exhibits profiles of streamwise and transverse power spectrum of water at the pipe centerline, which is calculated by using the Blackman-Tukey method. The ordinate is normalized by kinematic viscosity of water, ν, and dissipation rate of turbulence kinetic energy of water, $<\varepsilon_c>$, in single phase,

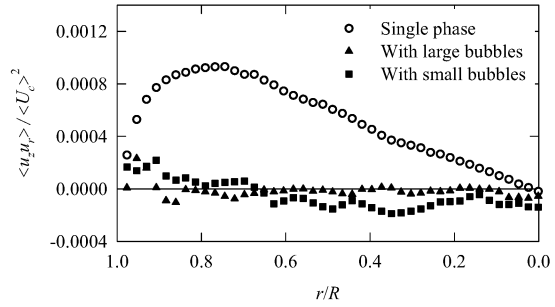

Figure 17. Profiles of the Reynolds stress in the presence of bubbles.

(*a*) Single phase (*b*) With large bubbles

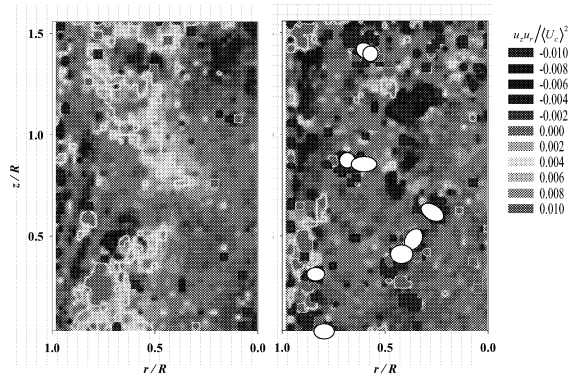

Figure 18. Contour plot of $u_z u_r$-correlation (*a*) in single phase and (*b*) in two phase with large bubbles.

while the abscissa is normalized by the Kolmogorov micro time scale of water, τ_κ, in single phase. It is found that turbulence energy in the high frequency region was increased and there is no significant difference between with and without surfactant. Significant augmentation was observed in the transverse power spectra in figure 16(*b*), which is mainly attributed to the transverse motion of bubbles due to the lift force, which is supported by large values of local void fraction near the wall as shown in figure 14.

Figure 17 shows profiles of the Reynolds stress, $<u_z u_r>$, in the presence of bubbles. Strong reduction was found in the whole region of pipe, which is not dependent on the bubble size. For further insight into flow structure around bubbles, the instantaneous velocity correlation, $u_z u_r$, was calculated for both single and two phases, as depicted in figure 18. The different structure is found in comparison with single phase as shown in figure 18(*a*), that is, the correlation has a tendency to show large positive and negative values in the vicinity of bubbles in figure 18(*b*). This trend yields positive and negative correlations be canceling each other out, which results in a reduction of the Reynolds stress.

The turbulence production and its dissipation rate of turbulence kinetic energy equation were calculated and plotted in profiles of energy budget as illustrated in figure 19. The ordinate is normalized by $<U_c>$ and kinematic viscosity. It is obvious that the turbulence production was deceased due to bubbles, however, its dissipation rate was significantly increased in the whole region of pipe. One can

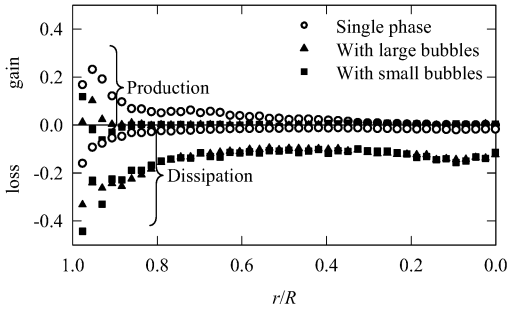

Figure 19. Profiles of energy budget of turbulence kinetic energy of water in the presence of bubbles. The ordinate is normalized by the mean streamwise velocity at the pipe centerline and kinematic viscosity.

see that the dissipation rate should be balanced with a term(s) in the turbulence kinetic energy equation, e.g., the pressure-velocity correlation term, thus further investigation will be carried out to validate the balance in equation.

Energy forward/backscatter by bubbles

The fluid velocities obtained from PIV measurements were filtered by using the top-hat filter, as described in equations (2) and (3). Figure 20 displays contour plot of the *real* SGS stress, τ_{zr}, in the presence of large bubbles with the filter width of Δ = 0.5–2.0 mm. Positive values are found behind bubbles, while negative regions have a tendency to show large values amongst bubbles with an increase in the filter width.

Figure 21 depict contour plot of energy flux to subgrid scale, Π, which is defined as equation (10), with the filter width of Δ = 0.5–2.0 mm. Energy forward/backscatter occurs significantly in the vicinity of bubbles, which is emphasized with increasing values of the filter width. This trend was not observed in the experiments of liquid-solid turbulent channel flow. This may be attributed to the local vortex structure generated by bubble motion, which is not found in the interactions between fluid turbulence and solid particles.

The important question, i.e., the effect of pressure fluctuation induced by bubble motion on the energy cascade from large eddies to dissipative ones, has been left unanswered in the past experiments and simulations to this day. Ongoing research program will be performed to measure the pressure fluctuation in a bubbly flow in order to investigate how bubble motion affects the energy transport in turbulence.

CONCLUSIONS

PIV measurements with a high time resolution have been used to investigate the turbulence structure in dispersed two-phase flows. The methodology has been developed in the present study was applied to a liquid-solid flow in a vertical downflow water channel and an upward bubbly flow in a pipe. High speed cameras whose frame rate is less than the Kolmogorov micro time scale were employed to capture the small scale of fluid turbulence. Fluid information obtained from both experiments was filtered to investigate the energy forward/backscatter in the

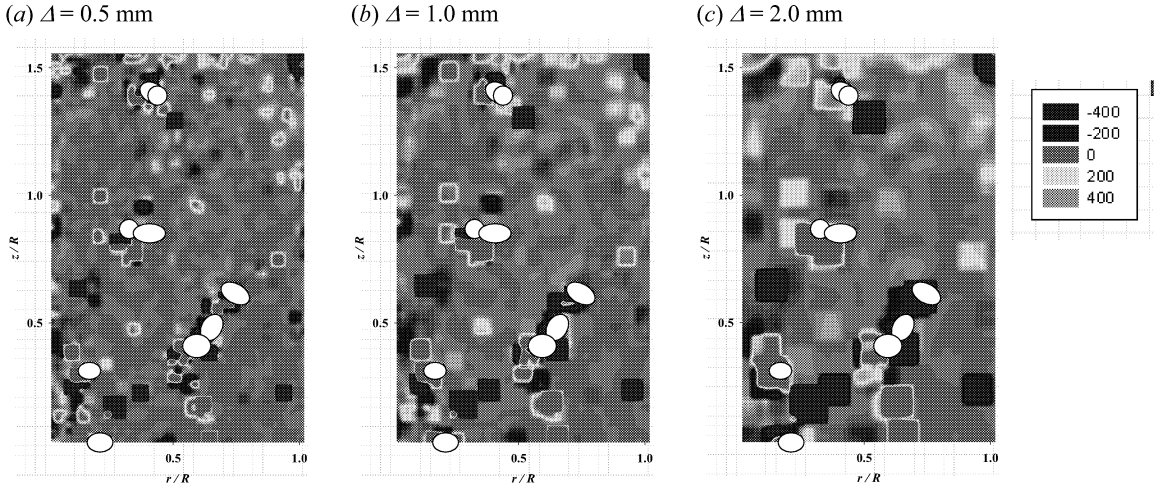

Figure 20. Contour plot of the *real* SGS stress element, τ_{zr}, computed with the top-hat filter of (*a*) $\Delta = 0.5$ mm, (*b*) $\Delta = 1.0$ mm and (*c*) $\Delta = 2.0$ mm.

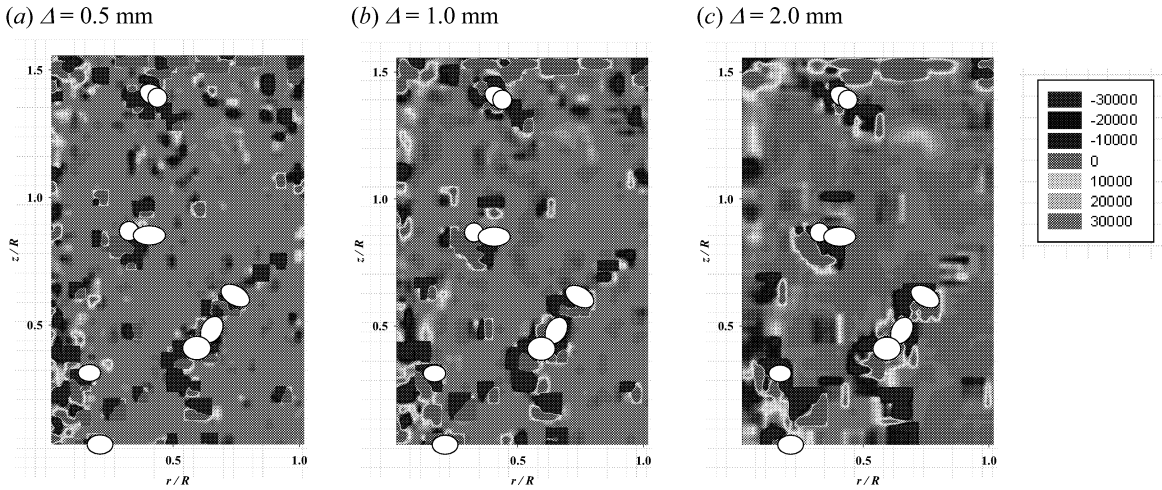

Figure 21. Contour plot of energy flux to subgrid scale, Π, computed with the top-hat filter of (*a*) $\Delta = 0.5$ mm, (*b*) $\Delta = 1.0$ mm and (*c*) $\Delta = 2.0$ mm.

presence of dispersed phase. The important conclusions obtained from this work are summarized below.

(1) Solid particles whose size is slightly greater than the Kolmogorov micro length scale enhanced fluid turbulence in a vertical channel flow. The turbulence intensity in the streamwise direction, which is identical to the gravity direction, was strongly augmented. The directional scale dependency structure was observed around particles, which is confirmed by the fact that large eddies were dissipated in front of particles and particle wave generated small eddies. This trend was emphasized when particles aligned perpendicular to the gravity direction.

(2) The SGS turbulence energy was increased until $\Delta/\eta \approx 10$ in the presence of particles, indicating that particles generate eddies whose size is less than 10η.

(3) The energy backscatter due to particles was significant at $\Delta/d_p \approx 5$, which is confirmed by results of the energy flux and the SGS dissipation rate obtained from PIV measurements. This result indicated that particles affected the eddy motion whose size is approximately five times particle diameter.

(4) Turbulence energy was augmented by both large and small bubbles in an upward pipe flow, which induced its dissipation rate in the whole region of pipe. Especially the transverse energy power spectra was increased by the transverse motion of bubbles due to the lift force.

(5) The instantaneous velocity correlation in the vicinity of bubbles showed both positive and negative values, which were canceled each other out. Thus the Reynolds stress was strongly reduced, which means that the dissipation rate should be balanced with other terms in the turbulence kinetic energy equation.

(6) The local vortex structure generated by bubble motion enhanced the energy forward/backscatter in the vicinity of bubbles, which is responsible for the energy transfer from large eddies to dissipative ones, and the energy supply from bubble motion.

ACKNOWLEDGEMENTS

The authors would like to thank Messrs. T. Tanaka, D. Minato and K. Yoshimura at Keio University for their performing experiments. The latter work of this study was carried out as one of the research activities at the Center for Smart Control of Turbulence funded by the Japanese

Ministry of Education, Culture, Sports, Science and Technology.

REFERENCES

Boivin, M., Simonin, O., and Squires, K.D., 1998, "Direct Numerical Simulation of Turbulence Modification by Particles in Isotropic Turbulence," *Journal of Fluid Mechanics*, Vol. 375, pp. 235–263.

Eaton, J.K., 1994, "Experiments and Simulations on Turbulence Modification by Dispersed Particles," *Applied Mechanics Review, Vol. 47, No. 6, Part2, part of "Mechanics USA 1994" (A.S. Kobayashi ed.)*, S44–S48.

Elghobashi, S.E., and Truesdell, G.C., 1993, "On the Two-Way Interaction between Homogeneous Turbulence and Dispersed Solid Particles. I: Turbulence Modification," *Physics of Fluids A*, Vol. 5, pp. 1790–1801.

Fleckhaus, D., Hishida, K., and Maeda, M., 1987, "Effect of Laden Solid Particles on Turbulent Flow Structure of a Round Free Jet," *Experiments in Fluids*, Vol. 5, pp. 323–333.

Gore, R.A., and Crowe, C.T., 1989*a*, "Effect of Particle Size on Modulating Turbulent Intensity," *International Journal of Multiphase Flow*, Vol. 15, pp. 279–285.

Gore, R.A., and Crowe, C.T., 1989*b*, "Effect of Particle Size on Modulating Turbulent Intensity: Influence of Radial Location," *Turbulence Modification in Dispersed Multiphase Flow, ASME-FED*, Vol. 80, pp. 31–35.

Hishida, K., and Sato, Y., 1999, "Turbulence Structure of Dispersed Two-Phase Flows (Measurements by Laser Techniques and Modeling)," *Multiphase Science and Technology*, Vol. 10, pp. 323–346.

Inoue, H., Sato, Y., and Hishida, K., 2001, "Directional Scale Dependency on Force Coupling for Dispersed Two-Phase Turbulent Flows," *Second International Symposium on Turbulence and Shear Flow Phenomena*, Vol. 2, pp. 99–104.

Kulick, J.D., Fessler, J.R., and Eaton, J.K., 1994, "Particle Response and Turbulence Modification in Fully Developed Channel Flow," *Journal of Fluid Mechanics*, Vol. 277, pp. 109–134.

Lance, M., and Bataille, J., 1991, "Turbulence in the Liquid Phase of a Uniform Bubbly Air-Water Flow," *Journal of Fluid Mechanics*, Vol. 222, pp. 95–118.

Liu, S. Katz, J., and Meneveau, C., 1999, "Evolution and modeling of subgrid scales during rapid straining of turbulence," *Journal of Fluid Mechanics*, Vol. 387, pp. 281–320.

Liu, S., Meneveau, C., and Katz, J., 1994, "On the Properties of Similarity Subgrid-Scale Models as Deduced from Measurements in a Turbulent Jet," *Journal of Fluid Mechanics*, Vol. 275, pp. 83–119.

Minato, D., Tanaka, T., Fujiwara, A., Hishida, K., and Maeda, M., 2003, "The Modification of Turbulence Structure in Bubbly Pipe Flow (Effect of Void Fraction and Bubble Diameter)," *The 6th ASME-JSME Thermal Engineering Joint Conference*, CD-ROM.

Rizk, M.A., and Elghobashi, S.E., 1989, "A Two-Equation Turbulence Model for Dispersed Dilute Confined Two-Phase Flows," *International Journal of Multiphase Flow*, Vol. 15, pp. 119–133.

Rogers, C.B., and Eaton, J.K., 1991, "The Effect of Small Particles on Fluid Turbulence in a Flat-Plate Turbulent Boundary Layer in Air," *Physics of Fluids A*, Vol. 3, pp. 928–937.

Sato, Y., Fukuichi, U., and Hishida, K., 2000, "Effect of Inter-Particle Spacing on Turbulence Modification by Lagrangian PIV," *International Journal of Heat and Fluid Flow*, Vol. 21, pp. 554–561.

Sato, Y., and Hishida, K., 1996, "Transport Process of Turbulence Energy in Particle-Laden Turbulent Flow," *International Journal of Heat and Fluid Flow*, Vol. 17, pp. 202–210.

Sato, Y., and Hishida, K., 2003, "Energy Transport Mechanisms in Particle-Laden Turbulent Water Channel Flow," *Third International Symposium on Turbulence and Shear Flow Phenomena*, Vol. 1, pp. 215–220.

Sato, Y., Hishida, K., and Maeda, M., 1996, "Effect of Dispersed Phase on Modification of Turbulent Flow in a Wall Jet," *ASME Journal of Fluids Engineering*, Vol. 118, pp. 307–315.

Sato, Y., Paris, A.D., Tanaka, T., and Hishida, K., 2001, "Evolution of Subgrid Scale by Particles in a Turbulent Channel Flow Obtained from Lagrangian Measurements," *Second International Symposium on Turbulence and Shear Flow Phenomena*, Vol. 1, pp. 295–300.

Serizawa, A., Kataoka, I., and Michiyoshi, I., 1975, "Turbulence Structure of Air-Water Bubbly Flow. II. Local Properties," *International Journal of Multiphase Flow*, Vol. 2, pp. 235–246.

Squires, K.D., and Eaton, J.K., 1990, "Particle Response and Turbulence Modification in Isotropic Turbulence," *Physics of Fluids A*, Vol. 2, pp. 1191–1203.

Theofanous, T.G., and Sullivan, J., 1982, "Turbulence in Two-Phase Dispersed Flows," *Journal of Fluid Mechanics*, Vol. 116, pp. 343–361.

Tokurhiro, A., Maekawa, M., Iizuka, K., Hishida, K., and Maeda, M., 1998, "Turbulent Flow Past A Bubble and Ellipsoid Using Shadow-Image and PIT Techniques," *International Journal of Multiphase Flow*, Vol. 24, pp. 1383–1406.

Yosimura, K., Minato, D., Tanaka, K., Sato, Y., and Hishida, K., 2004, "Turbulence Modification in Bubbly Upward Pipe Flow (Extraction of Microscopic Turbulent Structure by High Speed Time-Resolved PIV)," *Third International Symposium on Two-Phase Flow Modelling and Experimentation*, CD-ROM.